Sharpened VO$_2$ Phase Transition via Controlled Release of Epitaxial Strain

Daesu Lee,[†] Jaeseong Lee,[‡] Kyung Song,[§,⊥] Fei Xue,[‖] Si-Young Choi,[⊥,#] Yanjun Ma,[†] Jacob Podkaminer,[†] Dong Liu,[‡] Shih-Chia Liu,[∇] Bongwook Chung,[○] Wenjuan Fan,[‡] Sang June Cho,[‡] Weidong Zhou,[∇] Jaichan Lee,[○] Long-Qing Chen,[‖] Sang Ho Oh,[§,◆] Zhenqiang Ma,[*,‡] and Chang-Beom Eom[*,†]

[†]Department of Materials Science and Engineering, University of Wisconsin-Madison, Madison, Wisconsin 53706, United States

[‡]Department of Electrical and Computer Engineering, University of Wisconsin-Madison, Madison, Wisconsin 53706, United States

[§]Department of Materials Science and Engineering, Pohang University of Science and Technology, Pohang 37673, Korea

[‖]Department of Materials Science and Engineering, The Pennsylvania State University, University Park, Pennsylvania 16802, United States

[⊥]Department of Materials Modeling and Characterization, Korea Institute of Materials Science, Changwon 51508, Korea

[∇]Department of Electrical Engineering, University of Texas-Arlington, Arlington, Texas 76019, United States

[○]School of Advanced Materials Science and Engineering, Sungkyunkwan University, Suwon 16419, Korea

[◆]Department of Energy Science, Sungkyunkwan University, Suwon 16419, Korea

Ⓢ *Supporting Information*

ABSTRACT: Phase transitions in correlated materials can be manipulated at the nanoscale to yield emergent functional properties, promising new paradigms for nanoelectronics and nanophotonics. Vanadium dioxide (VO$_2$), an archetypal correlated material, exhibits a metal−insulator transition (MIT) above room temperature. At the thicknesses required for heterostructure applications, such as an optical modulator discussed here, the strain state of VO$_2$ largely determines the MIT dynamics critical to the device performance. We develop an approach to control the MIT dynamics in epitaxial VO$_2$ films by employing an intermediate template layer with large lattice mismatch to relieve the interfacial lattice constraints, contrary to conventional thin film epitaxy that favors lattice match between the substrate and the growing film. A combination of phase-field simulation, in situ real-time nanoscale imaging, and electrical measurements reveals robust undisturbed MIT dynamics even at preexisting structural domain boundaries and significantly sharpened MIT in the templated VO$_2$ films. Utilizing the sharp MIT, we demonstrate a fast, electrically switchable optical waveguide. This study offers unconventional design principles for heteroepitaxial correlated materials, as well as novel insight into their nanoscale phase transitions.

KEYWORDS: *Vanadium dioxide, epitaxial thin films, strain, metal−insulator transition, nanoscale visualization*
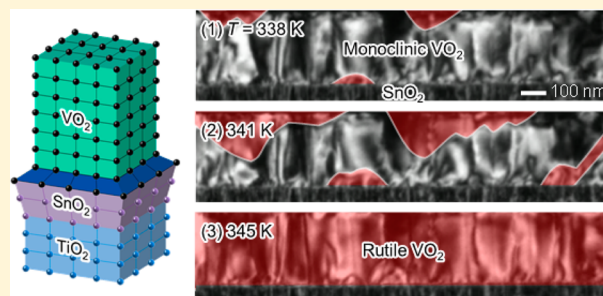
In correlated materials, charge−spin−orbital−lattice interactions have spawned a rich variety of electronic phases. Phase transitions between these various states provide building blocks for electronics and optoelectronics, as well as opportunities for discovering emergent phenomena including metal−insulator transition (MIT),[1] high-temperature superconductivity,[2] and colossal magnetoresistance.[3] One of the most fascinating and widely studied correlated materials is VO$_2$, which undergoes an MIT slightly above room temperature (i.e., $T_{MIT} \sim 341$ K in bulk).[4−12] In VO$_2$ single crystals, MIT shows a sudden jump in electrical resistivity by a factor of $\Delta\rho/\rho \geq 10^4$ and is also accompanied by a rutile−monoclinic structural phase transition [SPT; Figure 1a]. This sharp MIT above room temperature promises a wide range of potential applications, such as fast optoelectronic switches,[13,14] Mott transistors,[15]

memristors,[16] and artificial neuron networks.[17,18] Most of these applications require low-dimensional geometries such as thin films and deliberate control of MIT dynamics at the nanoscale, including phase nucleation and evolution. Until now, however, understanding and control of MIT dynamics in thin films have remained largely untouched.

Here, we report template engineering that utilizes an intermediate layer for growing epitaxial VO$_2$ films and controlling their nanoscale MIT dynamics. Thin-film growth of high-quality VO$_2$ (refs 19−23) has been attempted on rutile
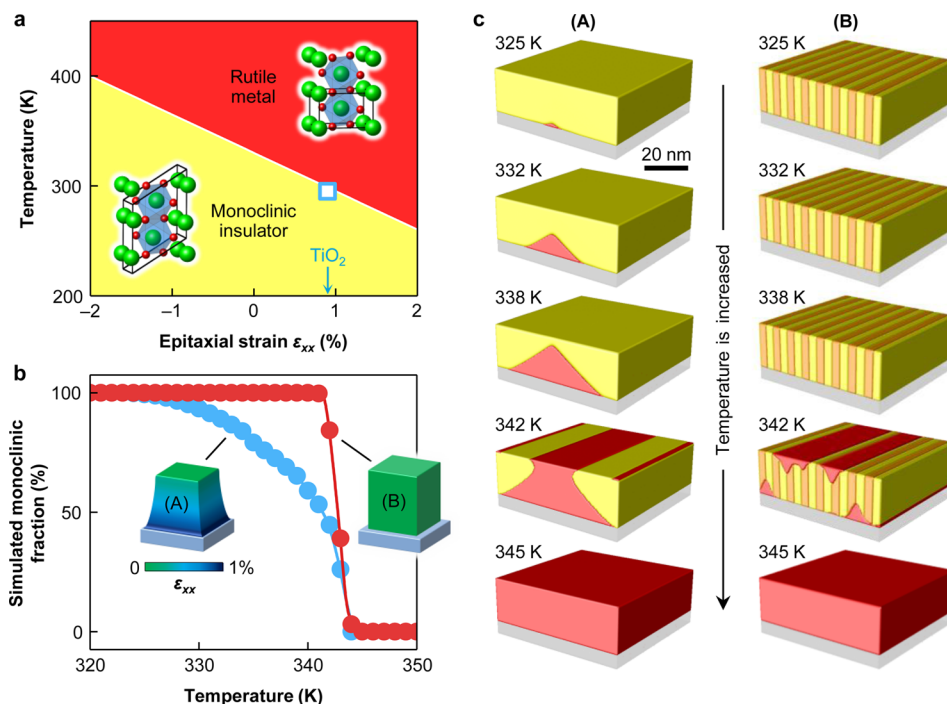
Figure 1. Theoretical prediction of phase transition dynamics in epitaxial VO_2. (a) Calculated strain-temperature phase diagram of a (001) VO_2 film. Epitaxial strain is defined as the relative change of in-plane lattice constant, that is, $(a_{film} - a_{bulk})/a_{bulk}$. Insets indicate atomic structures of monoclinic and rutile VO_2. The data point (blue square) shows the observed T_{MIT} of a coherent VO_2 film on (001) TiO_2. In fully coherent VO_2 films on (001) TiO_2, the epitaxial strain of ~0.9% lowers T_{MIT} down to ~290 K, which is undesirable for device operations at room temperature. (b) Simulated fraction of the monoclinic phase on heating in epitaxial VO_2 films with strain gradient [denoted by (A), corresponding to thick VO_2 films on (001) TiO_2] and with uniform bulklike lattice [denoted by (B)]. When films become thicker (i.e., ≥ 20 nm), the epitaxial strain starts to gradually relax and T_{MIT} broadens and approaches above room temperature. (c) Phase-field simulations of phase transition dynamics on heating for (A) and (B) cases in (b). Yellow and orange regions in (B) indicate two different monoclinic domains (Supporting Information, Figures S4 and S8), and red region denotes the rutile phase. Note the preferential nucleation at surface/interface in the (B) case due to the smaller nucleation energy barrier. Detailed simulation conditions are given in Supporting Information.

substrates,[19,21] such as TiO_2, due to the same crystal structure at growth temperatures. However, conventional epitaxial VO_2 films have suffered from lattice-strain-induced lowering[9,23] and/or broadening of T_{MIT} (Figure 1) and cracking[24] during SPT (Supporting Information, Figures S6 and S7), which limit their room-temperature device applications. Contrary to conventional thin-film epitaxy, which prefers a lattice-matched substrate or template,[25] we adopted the rutile SnO_2 template because of its large lattice mismatch (~4.2%) with VO_2. The huge lattice mismatch would lead to an incoherent interface with abrupt strain relaxation and uniform bulklike lattices in epitaxial VO_2 films, relieving the lattice constraint imposed by the substrate. Our theoretical simulation emphasizes that these conditions are essential for realizing sharp and homogeneous MIT dynamics at bulk T_{MIT} [Figure 1b,c, and Supporting Movies 1 and 2] and also preventing crack formation (Supporting Information, Figure S9). Thus, utilizing a template with a large lattice mismatch might control the MIT dynamics and could largely enhance the MIT in epitaxial VO_2.

We examined the lattice strain in VO_2 films, using X-ray diffraction reciprocal space mappings (RSMs). Figure 2c,d shows the RSMs around the TiO_2 (112) Bragg peak for VO_2 films on bare (001) TiO_2 and SnO_2-templated TiO_2, respectively. For VO_2/TiO_2 films [Figure 2c], the diffraction peak position of the film (yellow circle) was far from that of VO_2 bulk (blue star), indicating that the VO_2 film is still substantially strained. Furthermore, the diffraction peak of the film showed a streak pointing toward the bulk peak position,

implying a gradual strain relaxation in the film. In contrast, for $VO_2/SnO_2/TiO_2$ films [Figure 2d], the peak position of the film was identical to that of VO_2 bulk. This indicates that the use of the SnO_2 template enables the growth of unstrained epitaxial VO_2 films via abrupt strain relaxation at the interface.

To obtain further information, we conducted high-resolution, real-space strain mapping using dark-field inline electron holography [Figure 2e−h].[26] According to the measured strain map in VO_2/TiO_2 films [Figure 2e,g], the out-of-plane strain was around −1.8% near the bottom interface due to the misfit strain. The strain became relaxed and negligible near the top surface or cracks, which generates a strain gradient in both the out-of-plane and in-plane directions (Supporting Information, Figures S2 and S3). On the other hand, $VO_2/SnO_2/TiO_2$ films exhibited uniform bulk-like lattices without any crack or noticeable inhomogeneity [Figure 2f,h]. Notably, domain boundaries (Supporting Information, Figure S4) did not induce any considerable lattice inhomogeneity. On the basis of theoretical phase-field simulations [Figure 1b,c], these uniform bulklike lattices would lead to sharp and homogeneous MIT dynamics at bulk T_{MIT} in $VO_2/SnO_2/TiO_2$ films.

We used in situ transmission electron microscopy (TEM) to visualize the real-time phase transition dynamics in epitaxial VO_2 films (Supporting Movies 3 and 4). Figure 3a shows the monoclinic-to-rutile SPT dynamics in VO_2/TiO_2 films, according to which the rutile phase started to nucleate preferentially from the bottom interface (i.e., the highly strained region) at ~315 K, much lower than the bulk T_{MIT}
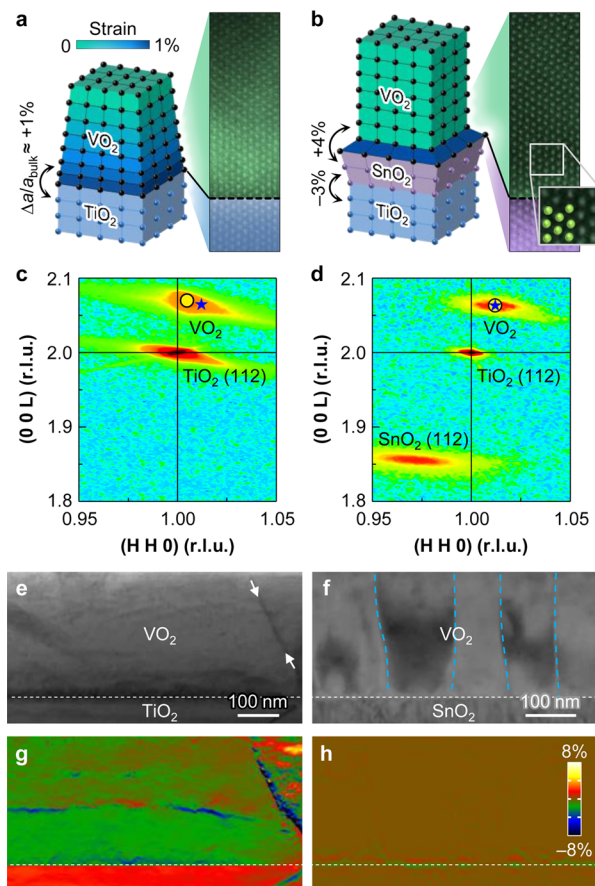
Figure 2. Design of uniform bulklike lattices in epitaxial VO$_2$. (a,b) Schematic diagrams showing the expected profile of lattice strain in epitaxial VO$_2$ films on (001) TiO$_2$ (a) without and (b) with SnO$_2$ template. Images on the right display the V atomic positions, obtained by low-angle annular dark-field imaging mode of scanning transmission electron microscopy near the bottom interface (see Supporting Information). (c,d) The X-ray RSM results around the TiO$_2$ (112) Bragg peak for 300 nm thick VO$_2$ films on (001) TiO$_2$ (c) without and (d) with SnO$_2$ template. The yellow circle and blue star indicate the peak position for the VO$_2$ film and bulk, respectively. (e,f) Bright-field TEM images for 300 nm thick VO$_2$ films on (001) TiO$_2$ (e) without and (f) with SnO$_2$ template. White arrows in (e) and blue dashed lines in (f) indicate cracks and domain boundaries, respectively. (g,h) Spatial maps for the out-of-plane lattice strain ε_{yy}, that is, ($c_{film} - c_{bulk}$)/c_{bulk}, in VO$_2$ films for the areas in (e,f).

($\sim$341 K). Then, the nucleated phase propagated toward the top surface and cracks. Both on heating (Supporting Movie 3) and cooling (Supporting Movie 4), the phase evolution nearly followed the measured profile of local strain [Figure 2g and Figure S3], consistent with theoretical simulations [Figure 1c]. This shows that local lattice strain determines the phase transition dynamics at the nanoscale and can explain why the phase transition of epitaxial VO$_2$ films usually proceeds over a wide range of T_{MIT}.

Differently from VO$_2$/TiO$_2$ films, however, VO$_2$/SnO$_2$/TiO$_2$ films showed a much sharper and homogeneous phase transition (Supporting Movie 5). Figure 3b shows that the rutile phase started to nucleate both from the top surface and bottom interface at $\geq$338 K, and then propagated forward, consistent with phase-field simulations [Figure 1c]. SPT was mostly completed in a narrow temperature range between $\sim$341 and $\sim$343 K. Quantitative analyses [Figure 3c] showed

more clearly that the phase transition occurred in a much narrower temperature range in VO$_2$/SnO$_2$/TiO$_2$ films than in VO$_2$/TiO$_2$ films. This highlights the fact that the use of a proper template can allow the sharp phase transition, as well as controlling the phase transition dynamics in epitaxial VO$_2$ films.

Interestingly, our in situ nanoscale imaging [Figure 3b] reveals that the propagating phase boundaries are not perturbed by the preexisting structural domain boundaries in the film but persist in continuous and collective evolution across such structural discontinuities. In conventional materials, structural discontinuities by domain or grain boundaries largely affect[27] and sometimes even inhibit phase transitions.[28] In epitaxial VO$_2$ films, however, domain boundaries do not disturb the propagation of phase boundaries (Supporting Information, Figure S8). This interesting feature might originate from the relatively large interfacial energy of phase boundaries. The monoclinic-to-rutile SPT in VO$_2$ is accompanied by a substantial change ($\geq$0.8%) in lattice parameters,[29] causing a large amount of elastic energy at phase boundaries between rutile and monoclinic phases. Furthermore, due to the coexisting SPT and MIT, phase boundaries in VO$_2$ have an electronic dissimilarity between insulating and metallic phases, which could further increase the phase boundary energy.[6] Thus, due to the smaller interfacial energy than phase boundaries, domain boundaries could have little effect during phase transition [as predicted in (B) of Figure 1b,c] and might not compromise the sharpness of phase transition.

Given the observed sharp and homogeneous SPT, we can naturally expect superb MIT in VO$_2$/SnO$_2$/TiO$_2$ films. The measured MIT showed resistivity change by a factor of $\sim$10^4 in VO$_2$/SnO$_2$/TiO$_2$ film [Figure 3d], whereas it became quite suppressed in VO$_2$/TiO$_2$ films due to the presence of cracks. Moreover, VO$_2$/SnO$_2$/TiO$_2$ films showed quite sharp MIT, whose transition width ΔT was as small as $\sim$0.7 K (Supporting Information, Figure S10). In the metallic phase, our VO$_2$/SnO$_2$/TiO$_2$ films showed not only low resistivity, but also a clear metallic characteristic (i.e., a decrease in resistivity with decreasing temperature), owing to the absence of severe structural/chemical defects in the film (Supporting Information, Figure S5). Furthermore, distinct from VO$_2$ single crystals[30] and conventional epitaxial films,[24] VO$_2$/SnO$_2$/TiO$_2$ films showed crack-formation-free MIT at bulk T_{MIT}, confirming excellent MIT features in VO$_2$/SnO$_2$/TiO$_2$ films.

We have shown that VO$_2$/SnO$_2$/TiO$_2$ films undergo abrupt MIT with varying temperature. Another possible and technologically more relevant way to trigger the MIT is to apply an external electric field.[5] Applying an electric field to VO$_2$ drives carrier injection, and then induces formation of a local metallic path in VO$_2$ on a short time scale of <1 ns.[31] However, after the metallic path forms locally, the electric field falls and a thermal process by Joule heating follows with the relation, $\Delta T \propto 1 - \exp(-t/\tau)$, where τ is a time constant.[31,32] When the electric field is removed, the reverse metal-to-insulator transition is also governed by a cooling process with $\Delta T \propto \exp(-t/\tau)$. These indicate that the switching speed in VO$_2$ could generally be limited to thermal processes (e.g., thermal transition width ΔT of MIT). Thus, the sharp MIT (i.e., narrow transition width ΔT) in VO$_2$/SnO$_2$/TiO$_2$ films would naturally allow a fast switching by electric field (i.e., small switching time Δt).

To evaluate the switching speed and potential device applications, we designed an electrically switchable optical waveguide, consisting of Si nanomembrane and epitaxial VO$_2$
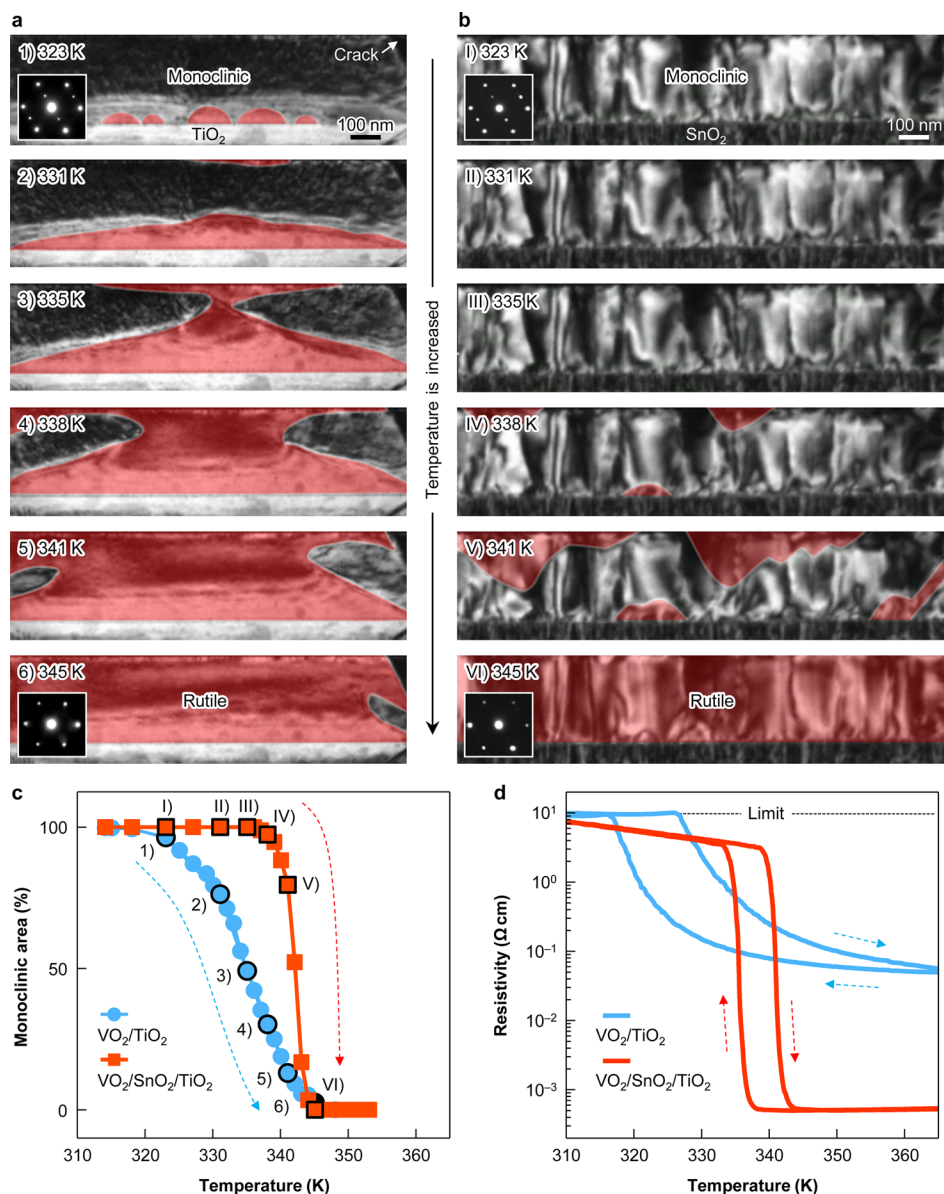
Figure 3. Nanoscale visualization and control of phase transition dynamics in epitaxial VO$_2$. (a,b) In situ TEM images during the monoclinic-to-rutile SPT on heating in 300 nm thick VO$_2$ films on (001) TiO$_2$ (a) without and (b) with SnO$_2$ template. The rutile phase is represented by red color. The temperature is ramped up at 5 K min^{-1} during these measurements. Insets in (a,b) indicate the measured nanobeam electron diffraction patterns of low-temperature monoclinic (upper) and high-temperature rutile (lower) phases for VO$_2$/TiO$_2$ and VO$_2$/SnO$_2$/TiO$_2$ films, respectively. (c) Monoclinic area as a function of temperature, determined from the in situ TEM images in (a,b). (d) Electrical resistivity as a function of temperature for VO$_2$ films.

film [Figure 4a and Figure S12]. During MIT, the optical constants of VO$_2$ (refractive index n and extinction coefficient k) become largely changed (Supporting Information, Figure S11).[14] Utilizing this, we can electrically control the mode confinement factor within the VO$_2$ film and therefore light transmission coefficient through a Si waveguide. When VO$_2$ is insulating (i.e., $n_{VO2} = 3.1$), light cannot be well propagated through a Si waveguide with $n_{Si} = 3.4$ due to imperfect total reflection and light absorption in VO$_2$ with $k_{VO2} = 0.3$ [Figure 4a,c]. On the other hand, when VO$_2$ is electrically switched to the metallic state (i.e., $n_{VO2} = 1.7$), the mode becomes tightly confined inside the Si waveguide such that the transmission loss substantially decreases [Figure 4b,d]. Importantly, while electrical transport measurements can be governed just by local metallic paths in VO$_2$, this optical transmission is

determined by the overall fraction of metallized VO$_2$, and thus can provide an effective way to estimate the genuine switching speed of VO$_2$ by electric field.

Figure 4e,f shows the time-dependent optical transmission upon the application and removal of an electric field for VO$_2$/TiO$_2$- and VO$_2$/SnO$_2$/TiO$_2$-based optical modulators. The light transmission became 10−100-times enhanced upon the application of an electric field, quantitatively consistent with our device simulations (Supporting Information, Figure S13). Regarding the switching speed, the VO$_2$/SnO$_2$/TiO$_2$-based device exhibited the full transition of light transmission on time scales of ∼150 and ∼300 ns during the on and off switchings, respectively [Figure 4f], which were 3−4 times shorter than those of VO$_2$/TiO$_2$-based devices [Figure 4e], and ∼10 times shorter than those of previously reported devices (i.e., a few
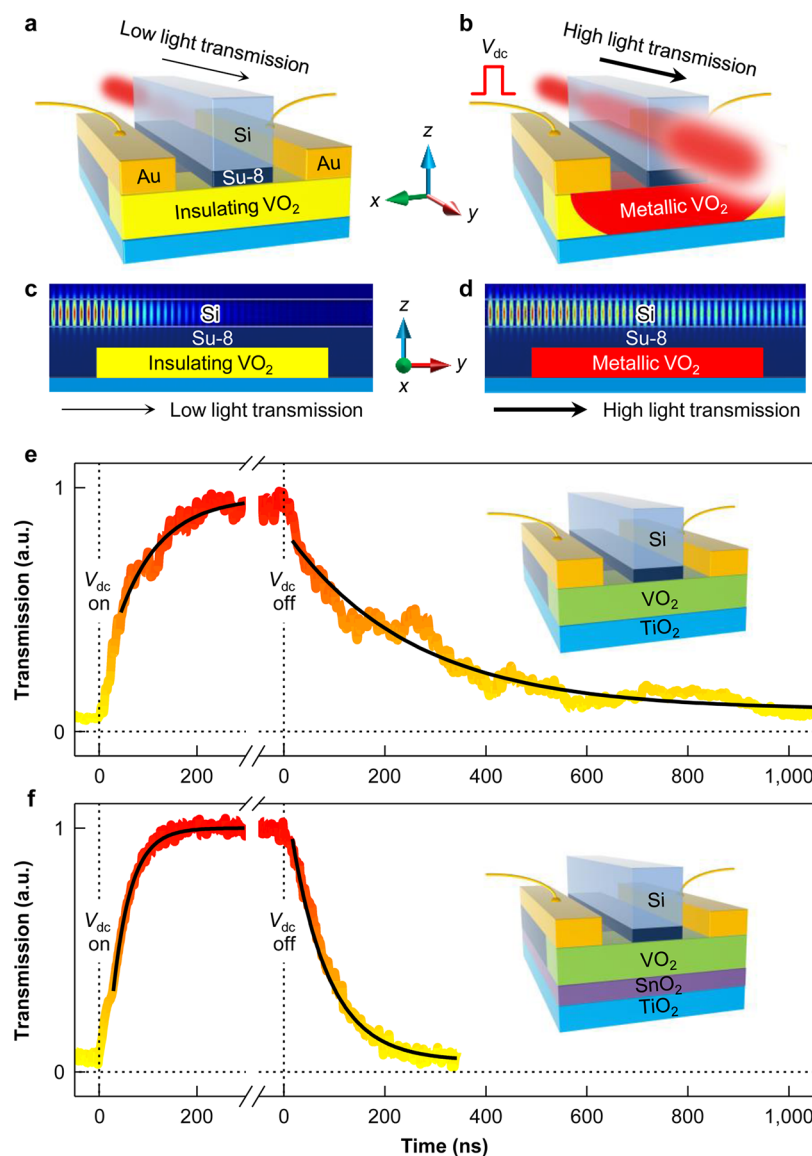
Figure 4. Electrically switchable optical waveguide using epitaxial VO₂. (a,b) Schematic drawings for the optical modulator consisting of single-crystal Si waveguide and epitaxial VO₂ film (a) without and (b) with applying an external voltage V_{dc}. We can metallize the VO₂ region by applying V_{dc}, which is higher than a threshold voltage for MIT. (c,d) Simulated light propagation through the Si waveguide for the light wavelength λ of 1.55 μm, when the VO₂ is in the (c) insulating and (d) metallic states. Fundamental TE-mode continuous-wave transmission through the Si waveguide is simulated by a finite-difference time-domain method, and electric-field intensity is captured. (e,f) Measured optical transmission as a function of time t for λ = 1.55 μm, when V_{dc} = 15 V is switched on and off for (e) VO₂/TiO₂- and (f) VO₂/SnO₂/TiO₂-based devices. The magnitude of transmission is also expressed in color from yellow (low transmission) to red (high transmission). Solid black lines are the fitted results with the formula of $1 - \exp(-t/\tau)$ and $\exp(-t/\tau)$.

microseconds).[14] By fitting, we estimated the time constant τ to be ~36 and ~74 ns during the on and off switching, respectively, for VO₂/SnO₂/TiO₂-based devices. In contrast, they were ~91 and ~252 ns during the on and off switching, respectively, for VO₂/TiO₂-based devices. The switching speed became greatly enhanced, possibly due to the sharp MIT of our SnO₂-templated films, but it could be further improved later by optimizing the device design.

We have demonstrated template engineering for epitaxial VO₂ films as a route for controlling and sharpening MIT at the nanoscale. Our study provides a nanoscale visualization of phase transition dynamics in epitaxial VO₂, which reveals not only the critical role of local lattice strain but also negligible effect of domain boundaries on MIT dynamics, contrary to conventional belief. This work opens up new avenues to

explore nanoscale phase transitions in correlated materials. Beyond MIT materials, it offers a general framework to design heteroepitaxial correlated materials with desired electronic functions.

■ ASSOCIATED CONTENT

ⓢ Supporting Information

The Supporting Information is available free of charge on the ACS Publications website at DOI: 10.1021/acs.nano-lett.7b02482.

Methods and additional figures (PDF)

Additional movies (ZIP)

Additional movie (AVI)

■ AUTHOR INFORMATION

Corresponding Authors
*E-mail: eom@engr.wisc.edu.
*E-mail: mazq@engr.wisc.edu.

ORCID 🟢
Jaichan Lee: 0000-0002-2730-9492
Chang-Beom Eom: 0000-0002-8854-1439

Present Address
#Department of Materials Science and Engineering, Pohang University of Science and Technology, Pohang 37673, Korea.

Author Contributions
The manuscript was written through contributions of all authors. All authors have given approval to the final version of the manuscript. D.L. and J.L. contributed equally.

Notes
The authors declare no competing financial interest.

■ REFERENCES

(1) Imada, M.; Fujimori, A.; Tokura, Y. *Rev. Mod. Phys.* **1998**, *70*, 1039−1263.
(2) Wu, M. K.; Ashburn, J. R.; Torng, C. J.; Hor, P. H.; Meng, R. L.; Gao, L.; Huang, Z. J.; Wang, Y. Q.; Chu, C. W. *Phys. Rev. Lett.* **1987**, *58*, 908−912.
(3) *Colossal Magnetoresistive Oxides*; Tokura, Y., Ed.; Gordon and Breach: London, 2000.
(4) Morin, F. J. *Phys. Rev. Lett.* **1959**, *3*, 34−36.
(5) Yang, Z.; Ko, C.; Ramanathan, S. *Annu. Rev. Mater. Res.* **2011**, *41*, 337−367.
(6) Nakano, M.; Shibuya, K.; Okuyama, D.; Hatano, T.; Ono, S.; Kawasaki, M.; Iwasa, Y.; Tokura, Y. *Nature* **2012**, *487*, 459−462.
(7) Liu, M.; Hwang, H. Y.; Tao, H.; Strikwerda, A. C.; Fan, K.; Keiser, G. R.; Sternbach, A. J.; West, K. G.; Kittiwatanakul, S.; Lu, J.; Wolf, S. A.; Omenetto, F. G.; Zhang, X.; Nelson, K. A.; Averitt, R. D. *Nature* **2012**, *487*, 345−348.
(8) Park, J. H.; Coy, J. M.; Kasirga, T. S.; Huang, C.; Fei, Z.; Hunter, S.; Cobden, D. H. *Nature* **2013**, *500*, 431−434.
(9) Aetukuri, N. B.; Gray, A. X.; Drouard, M.; Cossale, M.; Gao, L.; Reid, A. H.; Kukreja, R.; Ohldag, H.; Jenkins, C. A.; Arenholz, E.; Roche, K. P.; Dürr, H. A.; Samant, M. G.; Parkin, S. S. P. *Nat. Phys.* **2013**, *9*, 661−666.
(10) Jeong, J.; Aetukuri, N.; Graf, T.; Schladt, T. D.; Samant, M. G.; Parkin, S. S. P. *Science* **2013**, *339*, 1402−1405.
(11) Morrison, V. R.; Chatelain, R. P.; Tiwari, K. L.; Hendaoui, A.; Bruhács, A.; Chaker, M.; Siwick, B. J. *Science* **2014**, *346*, 445−448.
(12) Budai, J. D.; Hong, J.; Manley, M. E.; Specht, E. D.; Li, C. W.; Tischler, J. Z.; Abernathy, D. L.; Said, A. H.; Leu, B. M.; Boatner, L. A.; McQueeney, R. J.; Delaire, O. *Nature* **2014**, *515*, 535−539.
(13) Briggs, R. M.; Pryce, I. M.; Atwater, H. A. *Opt. Express* **2010**, *18*, 11192−11201.
(14) Joushaghani, A.; Jeong, J.; Paradis, S.; Alain, D.; Aitchison, J. S.; Poon, J. K. S. *Opt. Express* **2015**, *23*, 3657−3688.
(15) Newns, D. M.; Misewich, J. A.; Tsuei, C. C.; Gupta, A.; Scott, B. A.; Schrott, A. *Appl. Phys. Lett.* **1998**, *73*, 780−782.
(16) Driscoll, T.; Kim, H.-T.; Chae, B.-G.; Ventra, M. D.; Basov, D. N. *Appl. Phys. Lett.* **2009**, *95*, 043503.
(17) Pickett, M. D.; Medeiros-Ribeiro, G.; Williams, R. S. *Nat. Mater.* **2012**, *12*, 114−117.
(18) Zhou, Y.; Ramanathan, S. *Proc. IEEE* **2015**, *103*, 1289−1310.
(19) Muraoka, Y.; Hiroi, Z. *Appl. Phys. Lett.* **2002**, *80*, 583−585.
(20) Gupta, A.; Aggarwal, R.; Gupta, P.; Dutta, T.; Narayan, R. J.; Narayan, J. *Appl. Phys. Lett.* **2009**, *95*, 111915.
(21) Tashman, J. W.; Lee, J. H.; Paik, H.; Moyer, J. A.; Misra, R.; Mundy, J. A.; Spila, T.; Merz, T. A.; Schubert, J.; Muller, D. A.; Schiffer, P.; Schlom, D. G. *Appl. Phys. Lett.* **2014**, *104*, 063104.
(22) Zhang, H.-T.; Zhang, L.; Mukherjee, D.; Zheng, Y.-X.; Haislmaier, R. C.; Alem, N.; Engel-Herbert, R. *Nat. Commun.* **2015**, *6*, 8475.
(23) Quackenbush, N. F.; Paik, H.; Wahila, M. J.; Sallis, S.; Holtz, M. E.; Huang, X.; Ganose, A.; Morgan, B. J.; Scanlon, D. O.; Gu, Y.; Xue, F.; Chen, L.-Q.; Sterbinsky, G. E.; Schlueter, C.; Lee, T.-L.; Woicik, J. C.; Guo, J.-H.; Brock, J. D.; Muller, D. A.; Arena, D. A.; Schlom, D. G.; Piper, L. F. J. *Phys. Rev. B: Condens. Matter Mater. Phys.* **2016**, *94*, 085105.
(24) Paik, H.; Moyer, J. A.; Spila, T.; Tashman, J. W.; Mundy, J. A.; Freeman, E.; Shukla, N.; Lapano, J. M.; Engel-Herbert, R.; Zander, W.; Schubert, J.; Muller, D. A.; Datta, S.; Schiffer, P.; Schlom, D. G. *Appl. Phys. Lett.* **2015**, *107*, 163101.
(25) Lee, H. G.; Kim, Y.; Hwang, S.; Kim, G.; Kang, T. D.; Kim, M.; Kim, M.; Noh, T. W. *APL Mater.* **2016**, *4*, 126106.
(26) Koch, C. T. *Ultramicroscopy* **2008**, *108*, 141−150.
(27) Balluffi, R. W.; Allen, S. M.; Carter, W. C. *Kinetics of Materials*; John Wiley, 2005.
(28) Gao, P.; Britson, J.; Jokisaari, J. R.; Nelson, C. T.; Baek, S.-H.; Wang, Y.; Eom, C.-B.; Chen, L.-Q.; Pan, X. *Nat. Commun.* **2013**, *4*, 2791.
(29) Kucharczyk, D.; Niklewski, T. *J. Appl. Crystallogr.* **1979**, *12*, 370−373.
(30) Maurer, D.; Leue, A. *Mater. Sci. Eng., A* **2004**, *370*, 440−443.
(31) Ko, C.; Ramanathan, S. *Appl. Phys. Lett.* **2008**, *93*, 252101.
(32) Zimmers, A.; Aigouy, L.; Mortier, M.; Sharoni, A.; Wang, S.; West, K. G.; Ramirez, J. G.; Schuller, I. K. *Phys. Rev. Lett.* **2013**, *110*, 056601.